

# SSPFUSION: A SEMANTIC STRUCTURE-PRESERVING APPROACH FOR INFRARED AND VISIBLE IMAGE FUSION

Qiao Yang<sup>1</sup>, Yu Zhang<sup>2</sup>, Jian Zhang<sup>1,\*</sup>, Zijing Zhao<sup>1</sup>,  
Shunli Zhang<sup>1</sup>, Jinqiao Wang<sup>1</sup>, Junzhe Chen<sup>1</sup>

1. School of Software Engineering, Beijing Jiaotong University, China
2. School of Astronautics, Beihang University, China

## ABSTRACT

Most existing learning-based infrared and visible image fusion (IVIF) methods exhibit massive redundant information in the fusion images, i.e., yielding edge-blurring effect or unrecognizable for object detectors. To alleviate these issues, we propose a semantic structure-preserving approach for IVIF, namely SSPFusion. At first, we design a Structural Feature Extractor (SFE) to extract the structural features of infrared and visible images. Then, we introduce a multi-scale Structure-Preserving Fusion (SPF) module to fuse the structural features of infrared and visible images, while maintaining the consistency of semantic structures between the fusion and source images. Owing to these two effective modules, our method is able to generate high-quality fusion images from pairs of infrared and visible images, which can boost the performance of downstream computer-vision tasks. Experimental results on three benchmarks demonstrate that our method outperforms eight state-of-the-art image fusion methods in terms of both qualitative and quantitative evaluations. The code for our method, along with additional comparison results, will be made available at: <https://github.com/QiaoYang-CV/SSPFUSION>.

**Index Terms**— Image fusion, self-supervised learning, structure consistency

## 1. INTRODUCTION

To improve the ability of both human and computer vision systems to perceive their surrounding environment, multiple modalities of images, e.g., visible and infrared images, are frequently captured simultaneously to provide comprehensive information about the monitored scene [1]. Researchers have developed various methods to fuse the pairs of infrared and visible images as high-quality images, which can significantly enrich the image details and support the downstream computer-vision tasks (e.g., object tracking [2], multi-target detection [3], real-time semantic segmentation [4]). Intuitively, images fused from different modalities of images can comprehensively reflect conditions of the monitored scene.

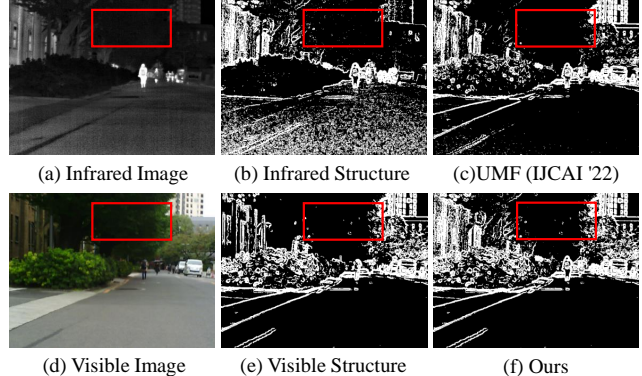


**Fig. 1.** A challenging IVIF image of (a) and (d), from MSRS, fused by SOTA method (c) and our method (f). As shown in the red box, our method can obtain robust cross-modal representation from the structure maps (b) and (e).

Recently, in order to produce high-quality fused images, many learning-based IVIF methods have been developed. These methods [5–10] implicitly utilize various loss functions to maximize the structural similarity between the fused and original images. However, these loss functions are primarily employed to manipulate gradient or color consistency rather than directly acting on the underlying structural consistency, which leads to redundant information in the fused image and low structural similarity between the fused and original images. Although some works [3, 11] pointed out that exploiting structural information could help improve the performance of IVIF methods, these methods encounter a challenge regarding structure inconsistency between the fused and source images. As shown in the red boxed Fig. 1, the tree structure is clearly showed in the visible image, but absent in the fused image of UMF [11].

To address the above issues, we propose a semantic structure-preserving approach for IVIF, namely SSPFusion. First, we design a Structural Feature Extractor (SFE) to extract structural features for the infrared and visible images and provide supervision signals for fused structures throughout the fusion process. Second, we develop a novel Structure-Preserving Fusion (SPF) module. With the supervision sig-

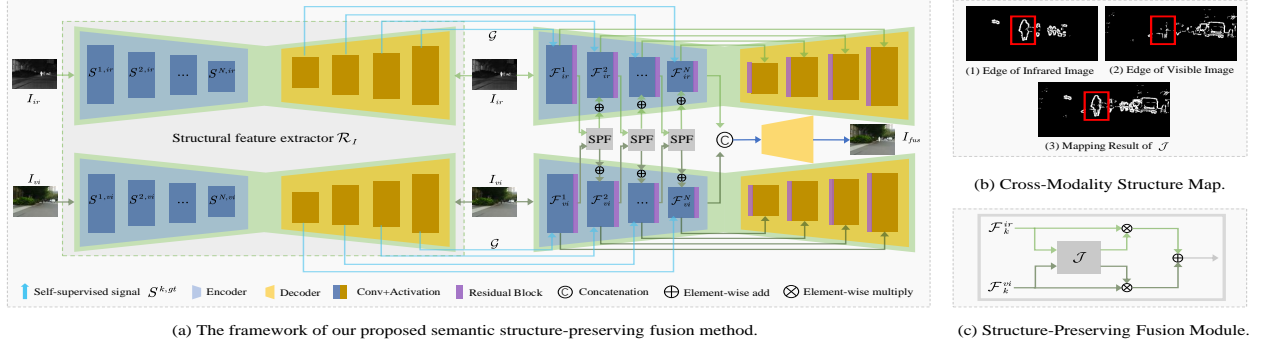


**Fig. 2.** (a) Flowchart of our proposed semantic structure-preserving fusion method. (b) Demonstration example of structure preservation. (c) Architecture of structure-preserving fusion module.

nals provided by SFE, SPF integrates the structural features of the source images, which are further reconstructed as a fusion image with well-preserved structures by the Decoder. Owing to the proposed SFE and SPF modules, our method can ultimately preserve the structural features from source images to the fusion image and generate high-quality fusion image, as shown in Fig. 1 (f). Finally, extensive experiments verify that our method outperforms eight state-of-the-art image fusion methods on three public datasets, and can significantly boost the performance of semantic segmentation tasks.

## 2. PROPOSED METHOD

As shown in Fig. 2 (a), the base architecture of our method is a common U-shape [12] model. Firstly, our SFE extracts structure maps as self-supervised signals. Then, guided by these signals, SPF fuses the complementary structures of infrared and visible images by a structure preserving mechanism. Finally, the fused image is reconstructed from the fused structural features by the Decoder. For simplicity, we denote the infrared, visible and fused images by  $I_{ir}$ ,  $I_{vi}$  and  $I_{fus}$ , respectively. Meanwhile, all images are converted to the YUV color space before inputting to the model.

### 2.1. Structural Feature Extractor

To effectively extract structural features from the infrared and visible images, a structural feature extractor (SFE) is designed in particular, as illustrated in Fig. 2 (a). In SFE, the feature maps  $\mathcal{F}_1, \dots, \mathcal{F}_N$  are extracted by the multi-layer encoder with a down-sampling operator in each layer. Besides, for each layer  $k \in [1, N]$ , we also generates the corresponding structure maps  $S^k$  of the input image  $I$  as

$$S^k = \mathcal{G}(\mathcal{R}_I(I)) \quad (1)$$

where  $\mathcal{R}_I$  denotes the SFE (without skip connection and residual block) for recovering structures of the input images  $I$ .  $\mathcal{G}$  denotes a transformation function in structure domain,

which is calculated by

$$S_{i,j}^k = \begin{cases} 1, & \nabla S_{i,j}^k - \mathcal{A} S_i^k \leq 0 \\ 0, & \text{else} \end{cases} \quad (2)$$

where  $S_{i,j}^k$  is the  $j$ th pixel of the  $i$ th structure map  $S_i^k$ ,  $\nabla$  and  $\mathcal{A}$  represent the sobel operator and global average pooling operator, respectively.

These multi-scale feature maps emphasize the edge regions, benefiting the representation of structural features in the fusion process. Further, in order to avoid losing the complementary structural features during the fusion process, we take  $S_{i,j}^{k,gt}$  as self-supervised signals for IVIF task, i.e., taking  $S_{i,j}^{k,gt}$  as the corresponding ground truth of  $S_{i,j}^k$ .

### 2.2. Structure-Preserving Fusion

As shown in the red boxes of Figs. 2 (b), the edge maps (generated by binarizing the images after applying the sobel filter) of infrared and visible images can reflect the object's structures from different views. Intuitively, an image integrating the complementary cross-modal structures of infrared and visible images will be helpful for boosting high-level vision tasks. To this end, we design an effective cross-modal structure-preserving fusion scheme. Specifically, we first extract the unique structures of  $S^{k,ir}$  and  $S^{k,vi}$  by:

$$\mathcal{M}^k = \mathcal{J}(S^{k,ir}, S^{k,vi}), \quad (3)$$

where  $\mathcal{J}(x, y) = (1 - x)y + (1 - y)x$ .  $\mathcal{M}^k$  will be 1 when only one of  $S^{k,ir}$  and  $S^{k,vi}$  equals to 1. Thus, Eq. (3) yields an edge map specifically delineating the unique structures of  $S^{k,ir}$  and  $S^{k,vi}$ , excluding any shared features between them. In fusion images of the conventional-deep-learning-based methods, these unique structures preserved from source images should be significantly less than those shared features.

Therefore, regions of feature maps (i.e.,  $S^{k,ir}$  and  $S^{k,vi}$ ) with unique structures should be enhanced appropriately. Specifically, in this work, we enhance them by:

$$\hat{S}^{k,ir} = S^{k,ir} + (1 - \mathcal{M}_{ir}^k) \mathcal{F}_{ir}^k + \mathcal{M}_{ir}^k \mathcal{F}_{ir}^k, \quad (4)$$

$$\hat{S}^{k,vi} = S^{k,vi} + \mathcal{M}_{ir}^k \mathcal{F}_{ir}^k + (1 - \mathcal{M}_{ir}^k) \mathcal{F}_{ir}^k. \quad (5)$$

In this manner, the image model could preserve more complete structural features from the source images into its fusion image, as shown in Fig. 2 (c). Finally, the fusion image  $I_{fus}$  with different modalities of structures is reconstructed from fused features by the Decoder.

### 2.3. Loss function

To train our network, we define a set of loss functions based on structure-aware behaviors of infrared and visible images. The total loss function of SSPFusion is defined as

$$\mathcal{L}_{total} = \alpha \mathcal{L}_{rec} + \mathcal{L}_{fus}, \quad (6)$$

where  $\alpha$  controls the trade-off between these two terms.

$\mathcal{L}_{rec}$  is a Charbonnier Loss [13], which is used to reconstruct distance between  $S$  and the structural ground truth  $S^{gt}$  and can be calculated as

$$\mathcal{L}_{rec} = \sqrt{\|S - S^{gt}\|^2 + \varepsilon^2}, \quad (7)$$

where  $\varepsilon$  is a constant. We explicitly utilize  $\mathcal{L}_{rec}$  as the regularization to constrain source regions and prevent critical information loss in the fusion process.

$\mathcal{L}_{fus}$  encourages fused images to maintain structure consistency from the source images and can be calculated as

$$\mathcal{L}_{fus} = \mathcal{L}_{ssim} + \mathcal{L}_{smooth} + \mathcal{L}_{grad}, \quad (8)$$

where  $\mathcal{L}_{ssim}$  is formulated as

$$\mathcal{L}_{ssim} = 1 - \frac{1}{2} (SSIM_{I_{fus}, I_{ir}} + SSIM_{I_{fus}, I_{vi}}), \quad (9)$$

where  $SSIM_{A,B}$  [14] calculates the structural similarity of images  $A$  and  $B$ .  $\mathcal{L}_{smooth}$  and  $\mathcal{L}_{grad}$  are two constraints for maintaining appearance and texture features from the source images to fused image and can be calculated as

$$\mathcal{L}_{smooth} = \|I_{fus} - \max(I_{ir}, I_{vi})\|_1, \quad (10)$$

$$\mathcal{L}_{grad} = \|\nabla I_{fus} - \max(\nabla I_{ir}, \nabla I_{vi})\|_1, \quad (11)$$

where  $\|\cdot\|_1$  and  $\max(\cdot)$  denotes the  $l_1$ -norm and elementwise-maximum selection operator, respectively.

## 3. EXPERIMENTS

### 3.1. Dataset and Implementation Details

We use three popular benchmarks, i.e., MSRS, M<sup>3</sup>FD and RoadScene, to verify the efficacy of our image fusion model. Specifically, MSRS dataset is used to train (1083 pairs) and test (361 pairs) our model, and RoadScene (60 pairs) is used for validation. To further verify the generalization ability of our model, we directly exploit it to fuse images of the RoadScene (70 pairs) and M3FD (20 pairs) datasets. Our model is trained on a computer platform with two NVIDIA RTX 3090 GPUs for 300 epochs, and size of input images is set

**Table 1.** Quantitative evaluation results on the MSRS dataset.

|      | MI           | SF            | AG           | VIF          | Qabf         | SSIM         |
|------|--------------|---------------|--------------|--------------|--------------|--------------|
| GTF  | 2.060        | 7.679         | 2.302        | 0.507        | 0.346        | 0.708        |
| DID  | 2.536        | 6.520         | 2.209        | 0.677        | 0.395        | 0.597        |
| AUIF | 1.986        | <u>9.945</u>  | <u>2.933</u> | 0.576        | 0.332        | 0.622        |
| RFN  | 2.545        | 6.488         | 2.312        | 0.702        | 0.426        | 0.853        |
| U2F  | 2.419        | 3.846         | 1.357        | 0.441        | 0.135        | 0.495        |
| DeF  | <u>3.113</u> | 8.281         | 2.701        | <u>0.755</u> | 0.540        | 0.955        |
| UMF  | 3.062        | 9.523         | 2.785        | <u>0.749</u> | 0.546        | <u>0.967</u> |
| TarD | 2.175        | 3.723         | 1.326        | 0.559        | 0.185        | <u>0.675</u> |
| Ours | <b>5.792</b> | <b>11.007</b> | <b>3.499</b> | <b>1.035</b> | <b>0.703</b> | <b>0.993</b> |

**Table 2.** Quantitative evaluation results on the M<sup>3</sup>FD dataset.

|      | MI           | SF            | AG           | VIF          | Qabf         | SSIM         |
|------|--------------|---------------|--------------|--------------|--------------|--------------|
| GTF  | 3.248        | 14.808        | 5.473        | 0.562        | <u>0.617</u> | 0.873        |
| DID  | 2.285        | 7.274         | 2.913        | 0.536        | 0.296        | 0.704        |
| AUIF | 2.489        | <b>16.847</b> | <b>6.336</b> | <u>0.759</u> | 0.616        | 0.885        |
| RFN  | 2.355        | 9.483         | 3.927        | 0.567        | 0.467        | 0.850        |
| U2F  | 2.440        | 3.774         | 1.603        | 0.340        | 0.088        | 0.458        |
| DeF  | 2.297        | 11.428        | 4.221        | 0.560        | 0.509        | 0.876        |
| UMF  | 2.596        | 11.657        | 4.344        | 0.691        | 0.599        | <u>0.963</u> |
| TarD | 3.997        | 5.453         | 1.960        | 0.563        | 0.137        | 0.692        |
| Ours | <b>6.064</b> | <u>15.905</u> | <u>5.948</u> | <b>0.860</b> | <b>0.711</b> | <b>0.967</b> |

**Table 3.** Quantitative evaluation results on the RoadScene dataset.

|      | MI           | SF            | AG           | VIF          | Qabf         | SSIM         |
|------|--------------|---------------|--------------|--------------|--------------|--------------|
| GTF  | 3.563        | 10.173        | 3.783        | 0.426        | 0.345        | 0.775        |
| DID  | 2.440        | 4.440         | 1.773        | 0.357        | 0.166        | 0.501        |
| AUIF | 2.337        | <u>11.651</u> | 4.226        | 0.448        | 0.333        | 0.740        |
| RFN  | 2.516        | 9.761         | <u>4.239</u> | 0.492        | 0.375        | 0.832        |
| U2F  | 2.233        | 3.859         | 1.791        | 0.358        | 0.151        | 0.496        |
| DeF  | 2.629        | 10.206        | 3.921        | 0.494        | 0.415        | <u>0.916</u> |
| UMF  | 3.428        | 10.851        | 4.069        | <u>0.616</u> | <u>0.466</u> | <b>0.929</b> |
| TarD | <u>3.857</u> | 9.929         | 4.080        | 0.591        | 0.389        | 0.816        |
| Ours | <b>4.789</b> | <b>12.406</b> | <b>4.516</b> | <b>0.685</b> | <b>0.473</b> | 0.887        |

to 256×256. Adam optimizer is used to optimize parameters of our model with momentum terms of  $\beta_1=0.9$  and  $\beta_2=0.999$ . The initial learning rate is 2e-4 and decreased by the cosine annealing delay. Obtained the structure map is pretrained in the same way, and it is only trained for 50 epochs. In all experiments,  $N$ ,  $\alpha$ , and  $\varepsilon$  are set to 3, 1/100, and 1, respectively.

### 3.2. Performance Analysis

We conduct experiments against eight state-of-the-art methods, including GTF [5], DIDFuse [6], RFN-Nest [8], AUIF [15], U2Fusion [16], DeFusion [17], UMF-CMGR [11] and TarDAL [3] to verify the efficacy of our method. For fair comparison, we fine-tune these models on the MSRS dataset. **Qualitative evaluation.** One comparison example has been



**Fig. 3.** Qualitative comparison of different methods on fusing the "FLIR\_05252" pair from RoadScene. Close-up views of areas within the green and red boxes were positioned in the bottom-left and bottom-right corners for better clarity in comparison.

**Table 4.** Comparison of segmentation results on MSRS.

| Metric: mIoU(%) |       |      |       |     |       |      |              |
|-----------------|-------|------|-------|-----|-------|------|--------------|
| Ir              | 0.625 | GTF  | 0.701 | RFN | 0.718 | UMF  | 0.717        |
| Vi              | 0.661 | DID  | 0.663 | U2F | 0.713 | Tard | 0.687        |
|                 |       | AUIF | 0.693 | DeF | 0.714 | Ours | <b>0.723</b> |

shown in Fig. 3. It can be seen that the fusion image of our SSPFusion is significantly better than those of other methods in terms of structure preservation, complement information and color fidelity. Since other methods fail to consider the structure consistency between the fused image and source images, their results exhibit strong edge blurring effect and loss of textures, as demonstrated by the signage area in red boxes and electrical poles in the green boxes in Fig. 3. On the other hand, as indicated by the purple boxes, when the same semantic structures exist in both the infrared and visible images, our method can explicitly preserve these features during the fusion process, robustly ensuring that no critical structures are lost in the fused image.

**Quantitative evaluation.** We use six metrics, i.e., MI [18], SF [19], AG [20], VIF [21], Qabf [22] and SSIM [14], to evaluate the quality of fusion images by different methods. The evaluation results have been listed in Tables 3-5, in which values in **bold** and underlined indicate the best and second-best results, respectively. As shown in the three tables, our method obtains greatest MI, VIF and SSIM, indicating our fusion images get higher information gain and maintain structural consistency against the source images. Additionally, our method also achieves competitive results on other metrics.

### 3.3. Performance on Semantic Segmentation Task

To explore the influence of our method on high-level vision tasks, we test its performance for semantic segmentation on the MSRS dataset. Specifically, we select DeeplabV3+ [23] as the baseline segmentation model, train the segmentation model on the MSRS dataset (trained on 976 images and tested on 361 images), and evaluate the model's performance by mean Intersection over Union (mIoU).

**Table 5.** Quantitative results of the ablation studies.

| Datasets  | SFE      | SPF      | MI           | VIF          | Qabf         | SSIM         |
|-----------|----------|----------|--------------|--------------|--------------|--------------|
| MSRS      | <b>X</b> | ✓        | 5.517        | 0.979        | 0.654        | <b>1.003</b> |
|           | ✓        | <b>X</b> | 5.386        | 0.962        | 0.635        | 0.969        |
|           | ✓        | ✓        | <b>5.792</b> | <b>1.035</b> | <b>0.703</b> | 0.993        |
| RoadScene | <b>X</b> | ✓        | 4.706        | 0.661        | 0.459        | 0.874        |
|           | ✓        | <b>X</b> | 4.453        | 0.650        | 0.434        | 0.868        |
|           | ✓        | ✓        | <b>4.789</b> | <b>0.685</b> | <b>0.473</b> | <b>0.887</b> |

**Implementation Details.** For DeeplabV3+, all the models were trained with both Dice and Cross-entropy loss, and optimized by SGD over 340 epochs with a batch size of 4. The first 100 epochs were trained by freezing the baseline with a batch size of 8. The initial learning rate was 7e-3 and decreased by the cosine annealing delay.

**Quantitative Comparison.** The results in Table 4 indicate our method outperforms other methods on the semantic segmentation task. SSPFusion can integrate the most semantic structures into its fusion images, thereby improving classification/segmentation accuracy compared to other methods.

### 3.4. Ablation Analysis

Finally, we design ablation experiments to verify the effectiveness of SFE and SPF modules on MSRS and M<sup>3</sup>FD datasets. MI, VIF, Qabf and SSIM are selected as the evaluation metrics. As shown in Table 5, when incorporating SFE and SPF modules, our SSPFusion can precisely extract complementary features from both infrared and visible images, and robustly generate the fused images.

## 4. CONCLUSION

In this paper, we propose a novel semantic structure-preserving approach for infrared and visible image fusion. Introducing structure-aware consistency operations during fusing multi-modal features ensures that the network can pay more attention on preserving the structural information while enhancing the visual quality of the fused image. Extensive experiments validate the effectiveness of the proposed method.

## 5. REFERENCES

- [1] Yu Zhang, Lijia Zhang, Xiangzhi Bai, and Li Zhang, “Infrared and visual image fusion through infrared feature extraction and visual information preservation,” *Infrared Phys. Techn.*, vol. 83, pp. 227–237, 2017.
- [2] Xingchen Zhang, Ping Ye, Henry Leung, Ke Gong, and Gang Xiao, “Object fusion tracking based on visible and infrared images: A comprehensive review,” *Inf. Fusion*, vol. 63, pp. 166–187, 2020.
- [3] Jinyuan Liu, Xin Fan, Zhanbo Huang, Guanyao Wu, Risheng Liu, Wei Zhong, and Zhongxuan Luo, “Target-aware dual adversarial learning and a multi-scenario multi-modality benchmark to fuse infrared and visible for object detection,” in *CVPR*, 2022, pp. 5792–5801.
- [4] Linfeng Tang, Jiteng Yuan, and Jiayi Ma, “Image fusion in the loop of high-level vision tasks: A semantic-aware real-time infrared and visible image fusion network,” *Inf. Fusion*, vol. 82, pp. 28–42, 2022.
- [5] Jiayi Ma, Chen Chen, Chang Li, and Jun Huang, “Infrared and visible image fusion via gradient transfer and total variation minimization,” *Inf. Fusion*, vol. 31, pp. 100–109, 2016.
- [6] Zixiang Zhao, Shuang Xu, Chunxia Zhang, Junmin Liu, Jiangshe Zhang, and Pengfei Li, “DIDFuse: Deep image decomposition for infrared and visible image fusion,” in *IJCAI*, 2020, pp. 970–976.
- [7] Yu Zhang, Yu Liu, Peng Sun, Han Yan, Xiaolin Zhao, and Li Zhang, “IFCNN: A general image fusion framework based on convolutional neural network,” *Inf. Fusion*, vol. 54, pp. 99–118, 2020.
- [8] Hui Li, Xiao-Jun Wu, and Josef Kittler, “RFN-Nest: An end-to-end residual fusion network for infrared and visible images,” *Inf. Fusion*, vol. 73, pp. 72–86, 2021.
- [9] Shiwei Wu, Kang Zhang, Xia Yuan, and Chunxia Zhao, “Infrared and visible image fusion by using multi-scale transformation and fractional-order gradient information,” in *ICASSP*, 2023, pp. 1–5.
- [10] Jun Yue, Leyuan Fang, Shaobo Xia, Yue Deng, and Jiayi Ma, “Dif-fusion: Towards high color fidelity in infrared and visible image fusion with diffusion models,” *arXiv:2301.08072*, 2023.
- [11] Di Wang, Jinyuan Liu, Xin Fan, and Risheng Liu, “Unsupervised misaligned infrared and visible image fusion via cross-modality image generation and registration,” in *IJCAI*, 2022, pp. 3508–3515.
- [12] Olaf Ronneberger, Philipp Fischer, and Thomas Brox, “U-net: Convolutional networks for biomedical image segmentation,” in *MICCAI*, 2015, pp. 234–241.
- [13] Wei-Sheng Lai, Jia-Bin Huang, Narendra Ahuja, and Ming-Hsuan Yang, “Fast and accurate image super-resolution with deep laplacian pyramid networks,” *IEEE Trans. PAMI*, vol. 41, no. 11, pp. 2599–2613, 2019.
- [14] Zhou Wang, A.C. Bovik, H.R. Sheikh, and E.P. Simoncelli, “Image quality assessment: from error visibility to structural similarity,” *IEEE Trans. IP*, vol. 13, no. 4, pp. 600–612, 2004.
- [15] Zixiang Zhao, Shuang Xu, Jiangshe Zhang, Chengyang Liang, Chunxia Zhang, and Junmin Liu, “Efficient and model-based infrared and visible image fusion via algorithm unrolling,” *IEEE Trans. CSVT*, vol. 32, no. 3, pp. 1186–1196, 2022.
- [16] Han Xu, Jiayi Ma, Junjun Jiang, Xiaojie Guo, and Haibin Ling, “U2Fusion: A unified unsupervised image fusion network,” *IEEE Trans. PAMI*, vol. 44, pp. 502–518, 2022.
- [17] Pengwei Liang, Junjun Jiang, Xianming Liu, and Jiayi Ma, “Fusion from Decomposition: A self-supervised decomposition approach for image fusion,” in *ECCV*, 2022, pp. 719–735.
- [18] Qu Guihong, Zhang Dali, and Yan Pingfan, “Information measure for performance of image fusion,” *Electron. Lett.*, vol. 38, no. 7, pp. 313—315, 2002.
- [19] A.M. Eskicioglu and P.S. Fisher, “Image quality measures and their performance,” *IEEE Trans. COMM*, vol. 43, no. 12, pp. 2959–2965, 1995.
- [20] Guangmang Cui, Huajun Feng, Zhihai Xu, Qi Li, and Yueteng Chen, “Detail preserved fusion of visible and infrared images using regional saliency extraction and multi-scale image decomposition,” *Opt. Commun.*, vol. 341, pp. 199–209, 2015.
- [21] Yu Han, Yunze Cai, Yin Cao, and Xiaoming Xu, “A new image fusion performance metric based on visual information fidelity,” *Inf. Fusion*, vol. 14, no. 2, pp. 127–135, 2013.
- [22] Costas S Xydeas, Vladimir Petrovic, et al., “Objective image fusion performance measure,” *Electron. Lett.*, vol. 36, no. 4, pp. 308–309, 2000.
- [23] Liang-Chieh Chen, Yukun Zhu, George Papandreou, Florian Schroff, and Hartwig Adam, “Encoder-decoder with atrous separable convolution for semantic image segmentation,” in *ECCV*, 2018, pp. 833–851.